Journal of the Korean Ceramic Society

한국세라믹학회지

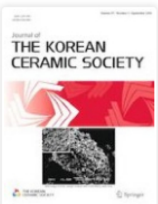

Volume 57, issue 5, September 2020

12 articles in this issue

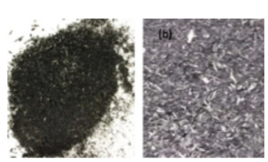

For authors

Submission guidelines

Ethics & disclosures

Fees and funding

Contact the journal

Submit manuscript

Explore

Online first articles

Volumes and issues

Sign up for alerts

Physico-mechanical behaviour of alkali and alkaline earth metal-containing mica glass–ceramics: a comparative evaluation

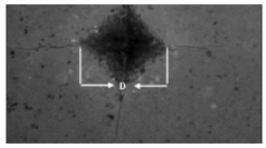

Amit Mallik

Original Article | Published: 07 May 2020 | Pages: 520 - 529

Influence of slag on mechanical and durability properties of fly ash-based geopolymer concrete

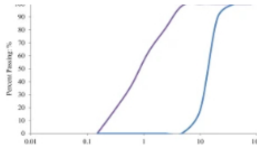

Ramamohana Reddy Bellum, Karthikeyan Muniraj & Sri Rama Chand Madduru

Original Article | Published: 20 May 2020 | Pages: 530 - 545

Geopolymer–carbonated apatite nanocomposites with magnesium and strontium trace elements for dental restorative materials

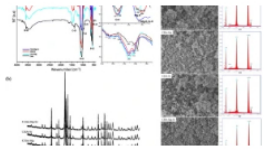

Dahlia Sutanto, Mieke Hemiawati Satari ... Bambang Sunendar Purwasasmita

Original Article | Published: 15 June 2020 | Pages: 546 - 556

Effect of magnetic particles adding into nanostructured hydroxyapatite–alginate composites for orthopedics

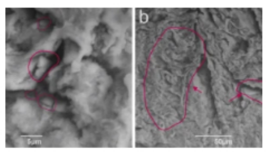

L. F. Sukhodub, L. B. Sukhodub ... D. Shokatayeva

Original Article | Published: 15 June 2020 | Pages: 557 - 569

Effect of $SrTiO_3$ modification on dielectric, phase transition and piezoelectric properties of lead-free $Bi_{0.5}Na_{0.5}TiO_3$–$CaTiO_3$–$SrTiO_3$ piezoelectric ceramics

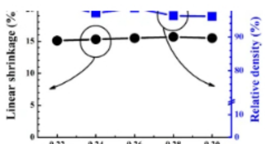

Hoang Thien Khoi Nguyen, Trang An Duong ... Jae-Shin Lee

Original Article | Published: 07 May 2020 | Pages: 570 - 577

Electro-caloric effects in the $BaTiO_3$-based solid solution ceramics

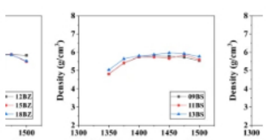

Bit Chan Kim & Chae Il Cheon

Original Article | Published: 20 May 2020 | Pages: 578 - 584

Surface modification and electrochemical performance of $KMnO_4$-ultra-surface area activated carbon (USAC) composites as cathode material

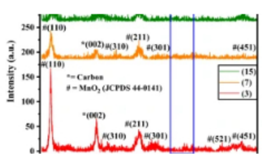

Zambaga Otgonbayar, K amrun Nahar Fatema ... Won-Chun Oh

Original Article | Published: 20 May 2020 | Pages: 585 - 596

Journal of the Korean Ceramic Society
https://doi.org/10.1007/s43207-020-00060-x

ORIGINAL ARTICLE

Geopolymer–carbonated apatite nanocomposites with magnesium and strontium trace elements for dental restorative materials

Dahlia Sutanto[1,2] · Mieke Hemiawati Satari[2] · Bethy S. Hernowo[3] · Bambang Pontjo Priosoeryanto[4] · Rifki Septawendar[5] · Lia A. T. W. Asri[6] · Bambang Sunendar Purwasasmita[7,8]

Received: 16 March 2020 / Revised: 12 May 2020 / Accepted: 16 May 2020

Abstract
Geopolymer and carbonated apatite are potential materials for dental restoration. We reported the synthesis of geopolymer–carbonated apatite nanocomposite, highlighting the influence of trace elements in carbonated apatite toward mechanical, leachability and cytotoxicity properties. Various carbonated apatites were combined with metakaolin, followed by geopolymerization. The study revealed that with addition of Mg^{2+} and Sr^{2+}, the geopolymer–carbonated apatite nanocomposites have the tendency to have lower mechanical properties. Geopolymer and geopolymer–carbonated apatite showed higher hardness, compressive strength, and modulus elasticity compared with geopolymer–carbonated apatite containing Mg^{2+} and/or Sr^{2+}. Nevertheless, all samples showed mechanical properties that could be applied as dental restoration materials. Leaching assay confirmed the release of Na^{+} in all samples, originating from unreacted alkali activator. The Na^{+} concentration decreased significantly after 96 h of total washing, with the lowest value of 1 ppm. Cytotoxicity test was evaluated toward mouse embryonic fibroblast cells, indicating that all samples were not toxic to cells.

Keywords Geopolymer · Carbonated apatite · Magnesium · Strontium · Dental restorative materials

1 Introduction

Ceramics are widely used as dental restoration to replace metal and metal–ceramic materials as they demonstrate high strength properties, biocompatibility, excellent translucency and toothlike color that contribute to highly esthetic restorations. Materials for dental restorations in oral environment are subjected to stress from mastication action, producing different reactions that lead to deformation, which can be ultimately compromised their durability over time. Ceramics can be also very hard and strong and capable of sustaining biting forces [1].

Geopolymers are ceramic-like inorganic polymers that are formed by dissolution and precipitation process of aluminosilicate precursor, such as thermally treated kaolin which are activated by alkaline solution [2]. They have excellent properties such as high compressive strength ranges from 52 to 75 MPa, durable, very small shrinkage and small creep,

✉ Dahlia Sutanto
dahlia.sutanto@dent.maranatha.edu

✉ Lia A. T. W. Asri
lia.asri@material.itb.ac.id

1 Faculty of Dentistry, Maranatha Christian University, Bandung 40164, Indonesia

2 Faculty of Dentistry, Department of Oral Biology, Padjajaran University, Bandung 40161, Indonesia

3 Faculty of Medicine, Department of Anatomical Pathology, Medical School Padjajaran University/Hasan Sadikin General Hospital, Bandung 40161, Indonesia

4 Faculty of Veterinary Medicine, Division of Veterinary Pathology, IPB University, Bogor 16680, Indonesia

5 Nanomaterials Research Group, Department of Advanced Ceramics, Glass, and Enamel, Center for Ceramics, Ministry of Industry of Indonesia, Bandung 40272, Indonesia

6 Materials Science and Engineering Research Group, Faculty of Mechanical and Aerospace Engineering, Bandung Institute of Technology, Bandung 40132, Indonesia

7 Advanced Materials Processing Group, Engineering Physics, Faculty of Industrial Technology, Bandung Institute of Technology, Bandung 40132, Indonesia

8 Research Center for Nanosciences and Nanotechnology, Bandung Institute of Technology, Bandung 40132, Indonesia

Published online: 15 June 2020

and high resistance to acid and sulfate corrosion [3–6]. Tippayasam et al. [7] reported the bioactive and biocompatible properties of geopolymers. They showed that geopolymers were able to accelerate the formation of new bone tissue by promoting the genetic activity of bone-regulating cells. Cataura et al. [8] reported the in vitro evaluation of metakaolin-based geopolymer which was suitable for hard tissue prostheses. Due to the mechanical and biological properties, geopolymers are potential materials that can be applied as indirect dental restoration.

Minerals in bones and teeth consist mostly of hydroxyapatite. In addition to Ca and PO_4^{3-}, various inorganic substances (CO_3^{2-}, Mg, Na, K, Sr, etc.) exist in bone minerals in the form of solid solution. Recently, the roles of these inorganic trace elements attract many interests [9]. Carbonate (CO_3^{2-}) is a biological apatite which is present in different amounts in bone (7.4 wt%), dentine (5.6 wt%), and enamel (3.5 wt%), where biological apatite is an inorganic calcium phosphate salt in apatite form and nano size with a biological derivation. Carbonate was shown to promote the formation of amorphous calcium phosphate [10]. Magnesium (Mg) and carbonate (CO_3^{2-}) are minor, but important elements associated with calcified tissues (enamel, dentine, bone) and diseased states (e.g., caries, osteoporosis). The level of Mg and CO_3^{2-} are higher in dentine and bone than in enamel apatite [10]. The presence of magnesium in calcified tissues was shown to inhibit the crystal growth of synthetic apatite, even promoting the formation of calcium phosphate at high concentration [10]. Strontium (Sr) is an essential trace element in the human body. There is a positive correlation between bone strength and Sr content. It is believed that Sr has an effect in preventing tooth decay [9, 11] and involved in antimicrobial activity [12]. Yang et al. [13] and Saidak et al. [14] reported that the presence of Sr resulted in enhanced osseointegration in vitro and in vivo.

Recent trends in technology focus on the incorporation of trace elements that extend the performance of materials. This paper is focused on the synthesis of geopolymer–carbonated apatite nanocomposites by varying magnesium and strontium trace elements. The mechanical properties and toxicity toward fibroblast cells were evaluated.

2 Experimental procedure

2.1 Materials

Sodium hydrogen carbonate, calcium nitrate tetrahydrate, diammonium hydrogen phosphate, magnesium chloride hexahydrate, strontium chloride hexahydrate, ammonia solution 25% and sodium hydroxide were purchased from Merck. Sodium silicate was obtained from Sigma-Aldrich. All reagents were of analytical grade and used without further purification. Kaolin was kindly provided by the Center for Ceramics, Ministry of Industry of Indonesia. Metakaolin was obtained by heating kaolin at 800 °C for 8 h in a furnace in air atmosphere.

2.2 Synthesis of carbonated apatite (CHA)

Ammonia solution was added dropwise to 100 mL of calcium nitrate tetrahydrate 0.1 M and stirred until pH reached 9, followed by addition of 100 mL of diammonium hydrogen phosphate 0.06 M and 100 mL of sodium hydrogen carbonate 0.06 M. Ammonia solution was added to adjust pH to 9. Solution was stored at RT for 12 h. The suspension was centrifuged at 8000 rpm. The precipitate was separated and dried in an oven at 80 °C for 30 min. The sample was then calcined at 700 °C for 2 h in air atmosphere. The final product was ground using a mortar, resulting in a fine white powder.

2.3 Synthesis of (Mg, Sr)-doped carbonated apatite

Five milliliters of $MgCl_2$ 0.01 M and $SrCl_2$ 0.01 M were prepared at pH 9. $MgCl_2$ or $SrCl_2$ or both the solutions were added into the solution containing calcium nitrate tetrahydrate, diammonium hydrogen phosphate and sodium hydrogen carbonate as mentioned in Sect. 2.2. Ammonia solution was added to adjust pH to 9. Precipitation of colloidal solution was done by keeping the solution at RT for 12 h. The sample was centrifuged at 8000 rpm. The precipitate was dried in an oven at 80 °C for 30 min. Heat treatment was done at 700 °C for 2 h in air atmosphere. The final product was ground using a mortar, resulting in a fine white powder.

2.4 Preparation of the geopolymer

The geopolymer sample was prepared by mixing metakaolin with alkali activator containing sodium silicate and 12 M NaOH with w/w ratio of 2:1. The resulting paste-like mixture was poured into an acrylic mold and stored at RT for 30 min and then dried in an oven at 80 °C for 20 h and samples were cooled to RT.

2.5 Preparation of geopolymer–CHA-(Sr, Mg) nanocomposites

CHA or CHA-(Sr, Mg) powder was mixed with metakaolin. Alkali activator containing sodium silicate and 12 M NaOH solution was added dropwise into the mixture powder sample and was blended to form a paste-like sample. Subsequently, the mixture was poured into an acrylic mold and stored at RT for 30 min and then dried in an oven at 80 °C for 20 h. The samples were cooled to RT.

2.6 Characterizations

FTIR measurements were recorded with KBr pellets on Prestige 21 Shimadzu. A sample shuttle measurement was performed to interleaved sample and background scan. The spectra were measured at a resolution of 4 cm^{-1} with the number of scans 40 and at wavelength 4500–400 cm^{-1}. The crystal structure was identified using X-ray diffraction (XRD) analysis, measured on Rigaku using Cu anode with wavelength of 1.5406 Å. The data were collected over the 2θ range of 15°–60°. The morphologies of CHA-(Mg, Sr) and geopolymer–CHA–(Mg, Sr) nanocomposites were observed using Hitachi SU3500 Scanning Electron Microscopy (SEM), operated at 10–15 kV. Sample compositions were measured using Hitachi SU3500 SEM-Energy Dispersive X-Ray Spectroscopy (EDX).

Hardness values of the samples were evaluated using HMV-G21 series Shimadzu Micro Vickers Hardness Tester. Indentation load was applied with F 100 gf and holding time 15 s. Nanocomposites specimens were prepared in cylinder of 5 mm diameter and 6 mm thickness. Each sample was indented on three different points. Diametral tensile strength and three points bending measurements were conducted using AGS-X series Shimadzu. Specimens for diametral tensile strength were prepared in a cylinder of 6 mm diameter and 3 mm thickness. The measurement was conducted with load cell F 1 kN, crosshead speed of 1 mm/s. Specimens for three points bending were prepared with bar of 25 mm × 5 mm × 2.0 mm with load cell 1 kN, 1 mm/s, and span of 10 mm. For the diametral tensile strength test, the specimens were compressed diametrically introducing tensile stress in the material in the plane of the force application by the test. This was obtained using Eq. (1) below [15].

$$\mathrm{DTS} = 2P/\pi DT \tag{1}$$

where DTS = diametral tensile strength, P = load applied, π = 3.14 (constant), D = diameter of the cylinder (mm), T = thickness of the cylinder (mm).

The modulus elasticity was obtained using Eq. (2) below [16]:

$$E = (P/d)\left(L^3/\left[4bh^3\right]\right) \tag{2}$$

where E = modulus elasticity, P = load at failure (N), d = slope in the linear elastic region of the load–displacement curve, L = length of specimen (mm), b = width of specimen (mm), h = thickness of specimen (mm).

Flexural strength was measured in a three-point flexure test which can be expressed using Eq. (3) below [17]:

$$S = 3P_{\max}L/\left(2bh^2\right) \tag{3}$$

where S = the maximum center tensile stress (MPa), P = the load at fracture (N), L = the distance of the two supports (mm), b = the width of the specimen (mm), h = the height of the specimen (mm).

The shrinkages of the samples were measured before (initial) and after (final) setting by measuring the change in dimension. Samples with rectangular shape with dimension of 35 mm × 5 mm × 2 mm ($l \times w \times t$) were measured at three different points, where l_0 = initial length (mm), l_t = final length (mm), w_0 = initial width (mm), w_t = final width (mm), t_0 = initial height (mm), and t_t = final height (mm).

2.7 Leaching test

Atomic Absorption Spectroscopy (AAS) was carried out to measure Na concentration that leached out from specimens during immersion in demineralized water. Each sample was washed with demineralized water for one minute before immersed in 100 mL of demineralized water, shaken at Thermo Fisher Scientific Compact Digital Mini Rotator H7KT26012 for 24 h. The leachate was collected, and sample was taken out. Sample was washed before immersed again in another 100 mL of demineralized water and was shaken at rotator for another 24 h. The leachate was collected every 24 with total washing time 96 h. The concentration of leaching Na was measured on AAS Agilent Technology 8453. Sample containing Na was diluted with demineralized water to the appropriate concentration. A series of Na standard solutions with various concentrations was prepared in demineralized water. Standard calibration curve was used to calculate the concentration of leaching Na.

2.8 Cytotoxicity assay of nanocomposites

Cytotoxicity assay was carried out using trypan blue method to verify the morphologies and viability of fibroblast cells. Samples were washed for 96 h in demineralized water before used. Fibroblast cells were initially cultured in RPMI 1640 medium (Gibco, USA). Samples were tested in the cylinder form with dimension of 3 mm diameter and 6 mm thickness. Samples were evaluated in duplicate. Fibroblast cells were plated at 100% cells/well in a 6-well plate and incubated for 24 h, 48 h, and 72 h at 37 °C. After incubation, all the culture mediums were aspirated into centrifuge tubes, each well was washed with 1 ml phosphate buffered saline pH 7.4 (Gibco, USA) and collected into centrifuge tubes. One ml of trypsin (Gibco, Denmark) was pipetted into each well and then incubated for 5 min. The incubated trypsin was aspirated and collected into each tube, cells were quantified by hemocytometer (Neubauer Improved, Marienfeld, Germany) and cells morphologies were analyzed using Motic Inverted Microscope (Olympus CK40) with 10 MP resolution camera [18, 19].

2.9 Statistical analysis

The mean value obtained from each group was used as a result and reported as mean ± standard derivation (SD). One-way analysis of variance (ANOVA) test was performed to assess the presence of any significant differences between the 5 study groups to the enamel and dentine. *p* values of less than 0.05 were considered statistically significant, followed by a post hoc 2-tail *p* values for pairwise independent groups *t*-tests with Excel MegaStat Software for statistical analysis.

3 Results and discussion

3.1 Synthesis of carbonated apatite

Figure 1a shows FTIR spectra of un-doped carbonated apatite (CHA), Mg (CHA-Mg), Sr (CHA-Sr) and Mg and Sr (CHA-Mg–Sr) doped carbonated apatite. These all types of apatites show similar profile at 3566 cm^{-1} indicating strong and sharp peak attributed to O–H stretching vibration of carbonated apatite [20, 21]. Peaks at 1014–1052 cm^{-1} and 659 cm^{-1} are attributed to P–O vibrations. Three characteristic carbonate bands at 1415, 1462 and 875 cm^{-1} are observed for all samples. All samples confirm the formation of both carbonated apatite type A and B as indicated by peak at 1417 cm^{-1} and 1412 cm^{-1}, originating from C–O vibration [21]. Apatite type B shows characteristic peaks at 1415 cm^{-1}. Addition of Mg and Sr dopants result in the change of type of apatite as shown by absorptions in the range 1700–1300 cm^{-1}. CHA sample shows peaks at 1462 cm^{-1}, 1412 cm^{-1} and 1384 cm^{-1}, while CHA-Mg, CHA-Sr and CHA-Mg–Sr samples demonstrate different peaks [21]. Addition of Mg and Sr dopants changes the absorption spectra in the range 450–420 cm^{-1}, while CHA shows no peaks in this area. CHA-Mg demonstrates peak at 433 cm^{-1} attributed to Mg–O vibration and CHA-Sr shows peak at 424 cm^{-1} attributed to Sr–O vibration. Mg and Sr dopants shifts the peak of metal oxide to 430 cm^{-1}, originating form overlapped Mg–O and Sr–O absorptions that appear as a broad peak with a shoulder.

The XRD patterns of all samples consist of a pure hydroxyapatite phase as according to PDF 2.841998. The hydroxyl apatite appearance in all CHA diffractograms is

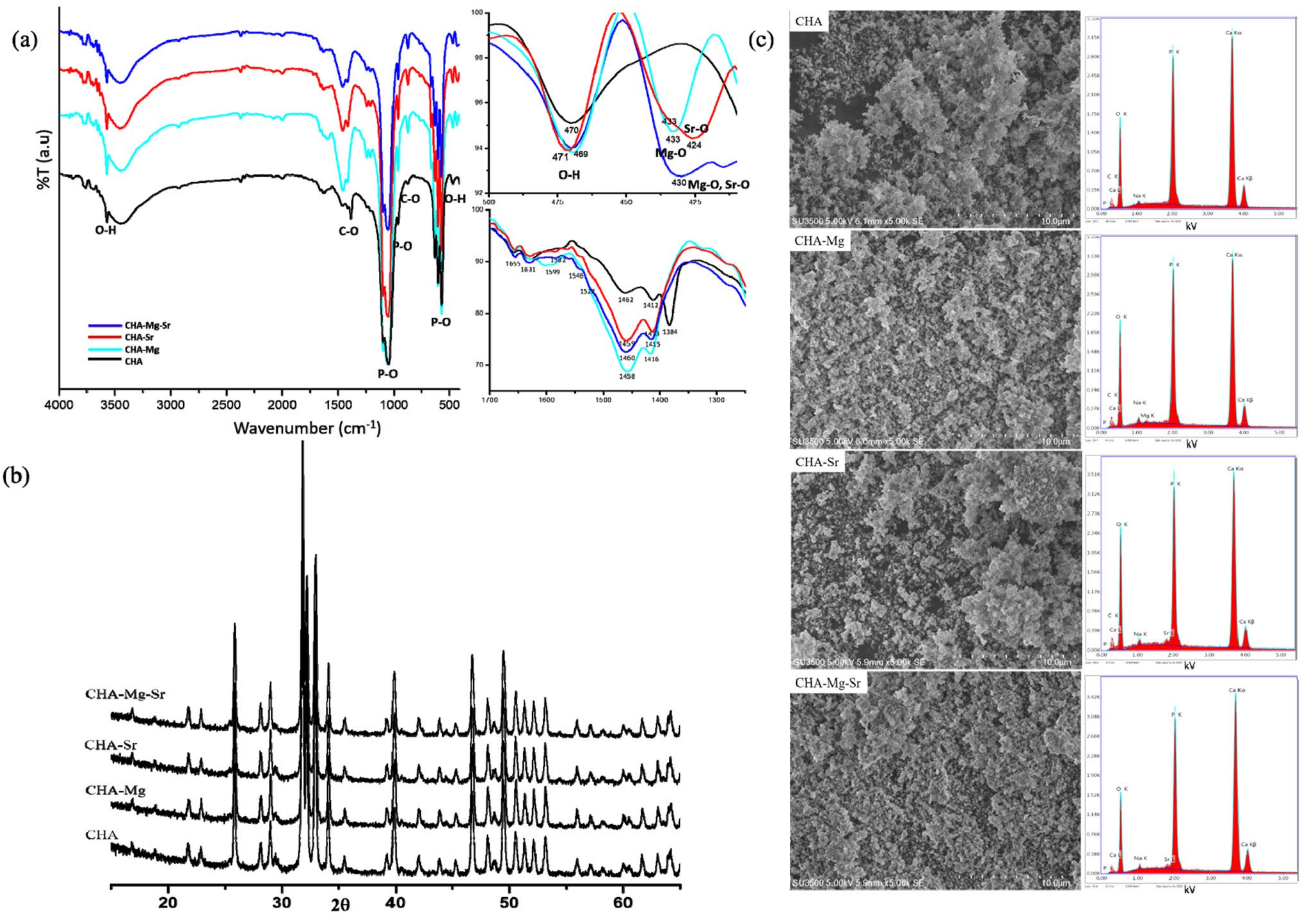

Fig. 1 **a** FTIR spectra, **b** XRD patterns, **c** SEM–EDAX spectra of CHA, CHA–Mg, CHA–Sr and CHA–Mg–Sr

shown by three main peaks of the hydroxyapatite phase at diffraction angles 2θ of 31.80°, 32.23°, and 32.96°, corresponding to the (121), (112), and (300) crystal planes of the hexagonal structures of hydroxyl apatite. However, the addition of Mg as a dopant into carbonated apatite resulted in the modification of the hydroxyapatite structures. These phenomena can be explained by the inexistence of the MgO peak in the sample diffractogram as shown in Fig. 1b and the increase in all hydroxyapatite peak intensities especially a peak at a diffraction angle 2θ of 46.77° which attributed to the (222) crystal plane of hydroxyapatite phase, as shown in Fig. 2. The absence of MgO peak in the CHA-Mg diffractogram indicates the formation of a solid solution of MgO as a dopant in the hydroxyapatite crystal structure. Nevertheless, the presence of MgO in the apatite sample is clearly detected by FTIR analysis, which identified the vibration

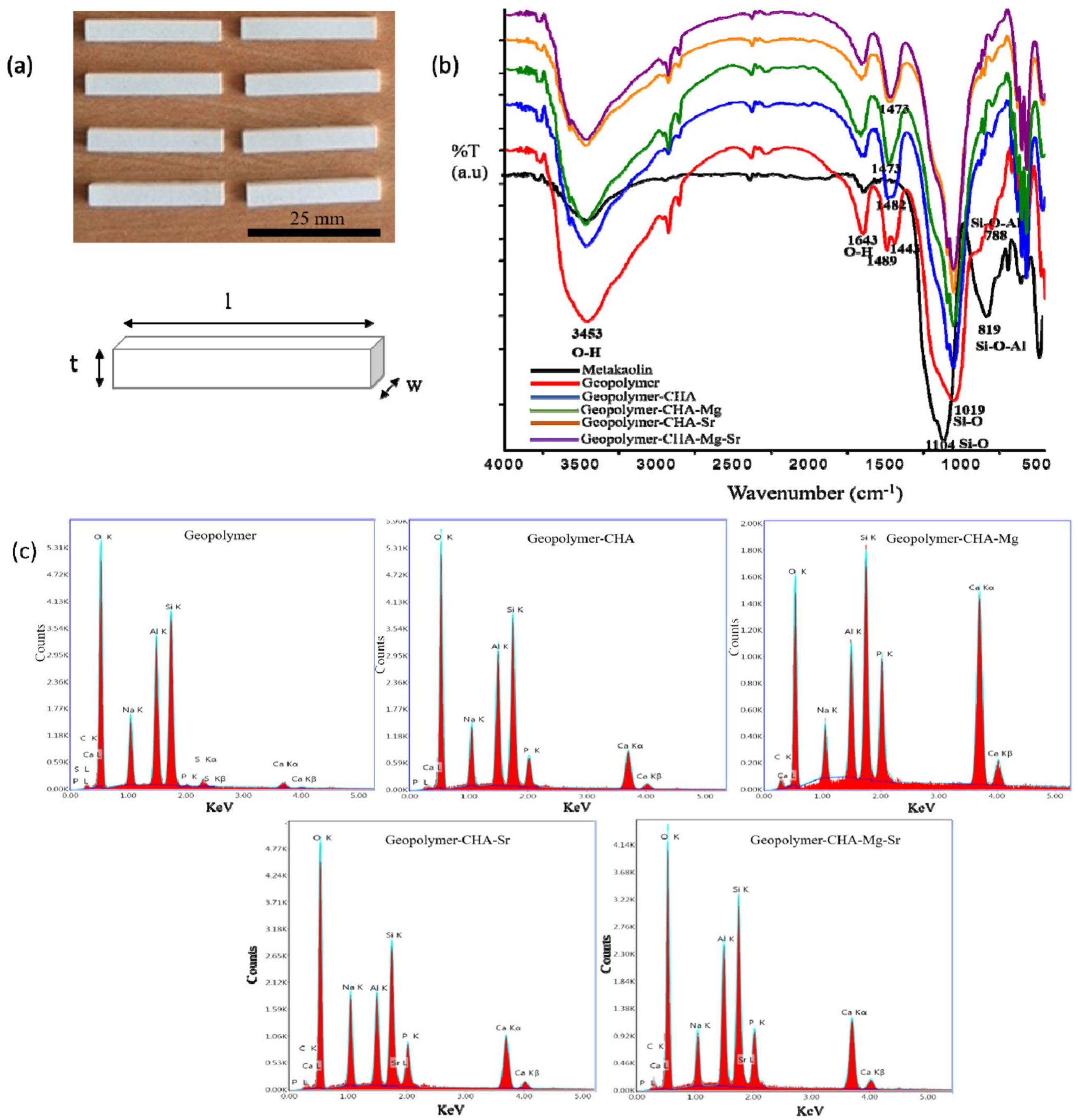

Fig. 2 **a** Nanocomposite specimens and illustration of the specimen dimensions for shrinkage test. **b** FTIR spectra and **c** EDAX spectra of various samples

mode of metal–oxygen of Mg–O in fingerprint area. The addition of MgO has also increased the formation of the hydroxyapatite (222) crystal plane in the hydroxyapatite structures compared to the pure CHA, which is shown by an increase in the peak intensity at a diffraction angle 2θ of 46.77°; thus this peak intensity has same level with a peak intensity at a diffraction angle 2θ of 49.50°, corresponding to the (123) crystal plane of hydroxyapatite phase. The presence of Sr_2O_3 as a dopant in the CHA-Sr sample does not give a significant change in the XRD results on the phase transformation of the apatite structure, which is in agreement with an XRD pattern standard of PDF 2.821429 for a Sr doped hydroxyapatite. The lack of Sr_2O_3 peak in the sample diffractogram suggests the formation of a Sr solid solution in the hydroxyapatite crystal structure. The presence of Sr_2O_3 in the sample has been confirmed by Sr–O absorption peak in FTIR analysis. Combination of MgO and Sr_2O_3 dopants in the carbonated apatite sample has shown the same phenomena with Sr_2O_3 in CHA-Sr sample in the XRD results. The dopants significantly increased all hydroxyapatite peak intensities especially a peak of the (222) crystal plane at a diffraction angle 2θ of 46.77°, as shown in Fig. 2b. It can be concluded that the MgO dopant plays more dominant than the Sr dopant in the hydroxyapatite structure modification.

SEM images of various carbonated apatite show formation of nanosized particles with some agglomerated particles. All samples demonstrate almost the same spherical morphologies (Fig. 1c). EDAX spectra reveal the presence of Mg and Sr trace elements added in carbonated apatite as shown in Fig. 1c, supporting the FTIR results. The EDAX spectrum of CHA-Mg–Sr only shows the small peak of Sr, while the peak of Mg is difficult to observe, however the FTIR spectrum indicates the Mg–O and Sr–O vibration. It can be concluded that Mg and Sr have been successfully incorporated into CHA.

3.2 Synthesis of geopolymer–carbonated apatite nanocomposites

Figure 2a displays geopolymer containing CHA nanocomposites after curing at 80 °C for 20 h. FTIR spectra in Fig. 2b confirm the formation of geopolymer in various cured samples. Geopolymerization of metakaolin results in a shift of Si–O from 1104 to 1019 cm^{-1}, while Si–O–Al vibration shifts from 819 to 788 cm^{-1} [22]. These shifts are correlated to the change in microstructure, due to the reorganization of the Si environment during the geopolymerization [23]. Peak at 3453 and 1643 in all samples containing geopolymer indicate the O–H stretching vibration from adsorbed water, whereas in metakaolin these peaks are relatively low. Geopolymer sample shows peaks at 1489 and 1443 cm^{-1} that indicate the formation of sodium carbonate because of the reaction between an excess of NaOH with CO_2 in the air.

The carbonated apatite, Mg and Sr trace elements are difficult to observe from FTIR, as most of the peaks are overlapped with geopolymer. The addition of carbonated apatite without and with the presence of trace elements shifts the two peaks at 1489 and 1443–1473 cm^{-1}, indicating the change in carbonate environment. A slightly change is observed at peak 1019 cm^{-1} (Fig. 2b), originating from Si–O–Si (tetrahedral bonds). The EDAX spectra confirm the incorporation of carbonated apatite as shown by the presence of Ca and P elements (Fig. 2c).

3.3 Leaching test

Geopolymerization of metakaolin was done by adding alkali activator, containing NaOH and sodium silicate. After reaction, unreacted NaOH or sodium silicate might remain in the samples and it can be toxic for oral environment. We carried out intensive washing steps in demineralized water to study the amount of Na^+ that leached out from specimens. Samples were tested after several washing steps. For each sample, every 24 h sample was taken out and then was immersed in the fresh demineralized water. Sampling of the Na^+ was done every 24 h with total washing time 96 h. Concentration of Na measured using AAS represented amount of Na^+ from unreacted alkali activator. Figure 3 shows amount of Na^+ decreases with the increase of washing time in all tested samples. After 24 h, Na^+ that were released from the specimens, accounted 56.19, 55.53, 50.16, 42.95 and 59.22 ppm for geopolymer, geopolymer–CHA, geopolymer–CHA–Mg, geopolymer–CHA–Sr and geopolymer–CHA–Mg–Sr respectively. After 48, 72 and 96 h of washing, the concentration of Na^+ decreased significantly. After 96 h of washing steps, the concentration of Na^+ reached 1–2.72 ppm with the lowest concentration

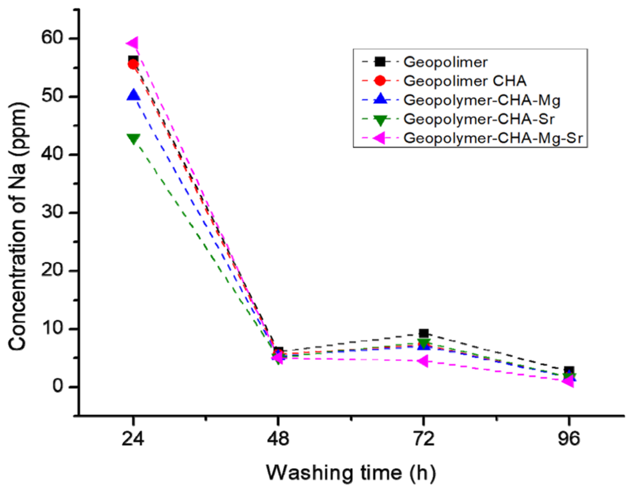

Fig. 3 Concentration of Na that leached out from various specimens after 24, 48, 72 and 96 h of washing steps

is shown by geopolymer–CHA–Mg–Sr sample. Tigue et al. [24] reported the leachability behavior of geopolymer-based fly ash. They showed a high concentration of Na^+ was attributed to high initial content of alkali activator. Aly et al. [25] reported that during the geopolymerization process, Al^{+3} takes on a coordination of 4, i.e., [Al(OH)4], and Na^+ maintains the charge balance in the geopolymer matrix. Once geopolymerization reaction was incomplete, excess Na^+ was deposited into the pores to form a saturated solution and some of it was accumulated on the geopolymer surface. Activation of geopolymer generally involves high concentration of alkali activator to increase the mechanical properties of the resulting materials. This result confirms that Na^+ from alkali activator did not react completely during geopolymerization. In our case, an intensive washing, at least 96 h of washing, is needed to be done before the geopolymer or modified geopolymer is applied as dental restoration.

3.4 Mechanical and shrinkage properties of geopolymer–carbonated apatite nanocomposites

The highest hardness value observed in the geopolymer group was 107.37 ± 15.22 VHN, while the geopolymer–CHA–Sr samples showed the lowest mean hardness value of 76.25 ± 5.25 VHN (Table 1). All samples demonstrated hardness values that had not yet reached the range of enamel value of 274.8 VHN, but they met the range of dentine value (53–63 VHN) [26, 27]. The compressive strength results showed the highest mean value was in the geopolymer–CHA group, while the lowest was in the geopolymer–CHA–Mg group. The compressive strength of all groups were higher than those in enamel (38.4–86 MPa), but lower than that of dentine (163.1–224.3 MPa) as presented in Table 1 [26, 27]. The highest average value of tensile strength was obtained by the geopolymer–CHA–Sr group and the lowest was shown by geopolymer–CHA–Mg–Sr. All groups presented higher tensile strength than the enamel value of 8–35 MPa, but lower than that of dentine (31–104 MPa) [26, 27] as summarized in Table 1.

Three points bending test was employed to determine the modulus elasticity and flexural strength of all samples. Geopolymer–CHA group reached the highest mean value of modulus elasticity and geopolymer–CHA–Sr group had the lowest. Higher modulus elasticity was revealed by the geopolymer and geopolymer–CHA group, which was higher than that of enamel (1030.3–1646.1 MPa), but lower than that of dentine (15.000 MPa) [26, 27]. The geopolymer–CHA group had the highest flexural strength, while geopolymer–CHA–Sr group showed the lowest value (Table 1).

A replacement material for enamel should have a hardness value similar to or lower than enamel and a replacement material for dentine should have modulus elasticity similar to or higher than dentine [28]. Compressive strength was considered as an indicator of success in resisting masticatory and parafunctional forces, while tensile strength was important as dental restorations are exposed to tensile stresses from transverse loading [29]. From mechanical properties point of view, all samples were good candidates as replacement material for enamel, while geopolymer–CHA was a good replacement material for enamel and dentine.

Doping Mg and Sr indeed affected the mechanical properties of the resulting nanocomposites. We observed that Sr showed higher effect in decreasing mechanical properties than Mg. The difference in phase formation in the hydroxyapatite structure between Sr and Mg dopant might affect the properties of CHA and further result in the change of the mechanical properties of nanocomposites. In addition, besides Ca^{2+} from CHA, Mg^{2+} and Sr^{2+} trace elements might be involved in the geopolymerization reaction [30], substituting Na^+ to be incorporated in the geopolymer network. FTIR spectra demonstrated a slight change at peak 1019 cm^{-1} (Fig. 2b), originating from Si–O–Si (tetrahedral bonds). In geopolymer–CHA containing Mg and Sr, this peak shifted to higher wavenumbers and appeared as a shoulder of the P–O peak from CHA. This shift indicates incorporation of alkaline earth cations [31]. Combination between Ca^{2+} from hydroxy apatite structure and trace elements might result in the change of bonds formed in geopolymers and further affect the mechanical properties of nanocomposites.

The shrinkage properties of the samples were evaluated by measuring the change in dimension of samples

Table 1 Mechanical properties of various samples

Sample	Hardness (VHN)	Compressive strength (MPa)	Tensile strength (MPa)	Flexural strength (MPa)	Modulus elasticity (MPa)
Geopolymer	107.37 ± 15.22	93.94 ± 8.87	12.71 ± 2.35	15.08 ± 0.57	10,325.22 ± 2616.76
Geopolymer–CHA	99.21 ± 19.35	102.85 ± 7.65	12.89 ± 1.65	20.71 ± 4.25	13,316.65 ± 1576.61
Geopolymer–CHA–Mg	96.95 ± 25.51	61.34 ± 8.89	12.05 ± 2.01	15.04 ± 0.67	9197.76 ± 2897.41
Geopolymer–CHA–Sr	76.25 ± 5.25	68.91 ± 13.25	15.03 ± 1.72	4.19 ± 1.05	3330.66 ± 467.78
Geopolymer–CHA–Mg–Sr	80.43 ± 11.36	71.21 ± 14.65	11.45 ± 3.40	11.29 ± 0.35	7193.04 ± 643.23

Table 2 Geopolymerization shrinkage of various nanocomposite samples

Sample	l_0 (mm)	l_t (mm)	w_0 (mm)	w_t (mm)	t_0 (mm)	t_t (mm)
Geopolymer	35	34.31 ± 0.37	5	5.03 ± 0.02	2	2.19 ± 0.08
Geopoymer–CHA	35	33.98 ± 0.10	5	5.00 ± 0.09	2	2.37 ± 0.09
Geopolymer–CHA–Mg	35	34.07 ± 0.08	5	4.99 ± 0.02	2	2.37 ± 0.07
Geopolymer–CHA–Sr	35	33.90 ± 0.15	5	5.00 ± 0.03	2	2.43 ± 0.05
Geopolymer–CHA–Mg–Sr	35	33.98 ± 0.10	5	5.05 ± 0.03	2	2.32 ± 0.06

before and after setting (Table 2). Samples with rectangular shape with dimension of 35 mm × 5 mm × 2 mm ($l \times w \times t$) were employed as shown in Fig. 2c. One-way ANOVA test showed the presence of significant different shrinkage in length between the five study samples with p values 0.0264, which were less than 0.05 and considered statistically significant. A post hoc two-tailed p values for pairwise independent groups t tests showed significant different shrinkage in length between geopolymer–CHA–Sr and geopolymer with p value 0.0486. One-way ANOVA test showed the presence of significant differences shrinkage in width between the five study groups with p values 0.0079. A post hoc two tail p values for pairwise independent groups t tests showed significant shrinkage differences in width between geopolymer-CHA-Mg and geopolymer with p value 0.0199, while geopolymer-CHA-Mg and geopolymer-CHA-Mg-Sr showed p value 0.0125. There was a strong significant difference between geopolymer–CHA and geopolymer with p value 0.0072, and geopolymer–CHA and geopolymer–CHA–Mg–Sr with p value 0.0079. One-way ANOVA test demonstrated the presence of significant differences shrinkage in samples height between the five study groups with p values 0.0008. A post hoc two-tail p values for pairwise independent groups t-tests showed that significant differences shrinkage in height between geopolymer and geopolymer–CHA–Mg–Sr with p value 0.0194, geopolymer and geopolymer–CHA with p value 0.0126, geopolymer–CHA–Mg–Sr and geopolymer–CHA–Sr with p value 0.0227. A strong significant difference was obtained between geopolymer and geopolymer–CHA–Mg with p value 0.0045 and between geopolymer and geopolymer–CHA–Sr with p value 0.0007. The highest shrinkage value was shown by sample length. This shrinkage might be due to the geopolymerization that is carried out at elevated temperature (80 °C). Geopolymerization can also be done at RT to prevent this shrinkage; however, it takes a longer setting time compared to the reaction at elevated temperature.

It can be concluded that mechanical property tests show that all samples reached the compressive, diametral tensile strength and modulus elasticity values of enamel, while the hardness values were lower than that of enamel but higher than that of dentin. All samples can be considered as good candidates for dental restoration.

3.5 Cytotoxicity test

Cytotoxicity test was carried out to verify the morphologies and viability of fibroblast cells after contact with various nanocomposite samples. The morphologies of fibroblasts after various incubation times, displayed in Fig. 4, show negligible alterations to the cell morphology or number, clearly indicating that it is not cytotoxic in nature. After 24, 48 and 72 h of growth, fibroblast showed good spreading, although some round-shaped fibroblasts were still observed.

The cell viability of the five samples are presented in Fig. 5. One-way ANOVA test showed that there were no significant differences between the five samples after 24 h, 48 h and 72 h of incubation, with p value more than 0.05. The statistically calculated p values were 0.4111, 0.4660 and 0.9523 for samples after 24 h, 48 h and 72 h, which were considered not statistically significant.

Cell viability of all samples showed a value higher than 80%. It is noteworthy to mention here that apparently all samples were biocompatible. After 72 h incubation, the cell viability reached higher than 90%, calculated 92.6% for geopolymer, 94.5% for geopolymer–CHA, 92.1% for geopolymer–CHA–Mg, 95.7% for geopolymer–CHA–Sr and 95.7% for geopolymer-–CHA–Mg–Sr. The sample containing Sr had the highest cell viability value after 72 h. Addition of trace elements might affect the cell viability, but it was statistically insignificant.

Geopolymer–CHA–Sr generally showed higher cell viability compared with geopolymer, geopolymer–CHA and geopolymer–CHA–Mg. In contrast geopolymer-CHA-Mg resulted in the lowest cell viability compared with other samples. Sr is an essential element in the human body. It has been reported that Sr showed antimicrobial activity and enhanced osseointegration in vitro and in vivo [12]. Addition of Sr trace element in samples might affect the dental restorative that requires high tissue integration. However, a further work is needed to be carried out to prove the effect of trace elements in geopolymer–carbonated nanocomposites.

Tippayasam et al. [7] reported that geopolymers showed biocompatibility properties, and were able to accelerate the formation of new bone–tissue by promoting the genetic activity of bone-regulating cells. Cataura et al. [2] also reported that metakaolin-based geopolymers were suitable for hard tissue prostheses. The development of geopolymers

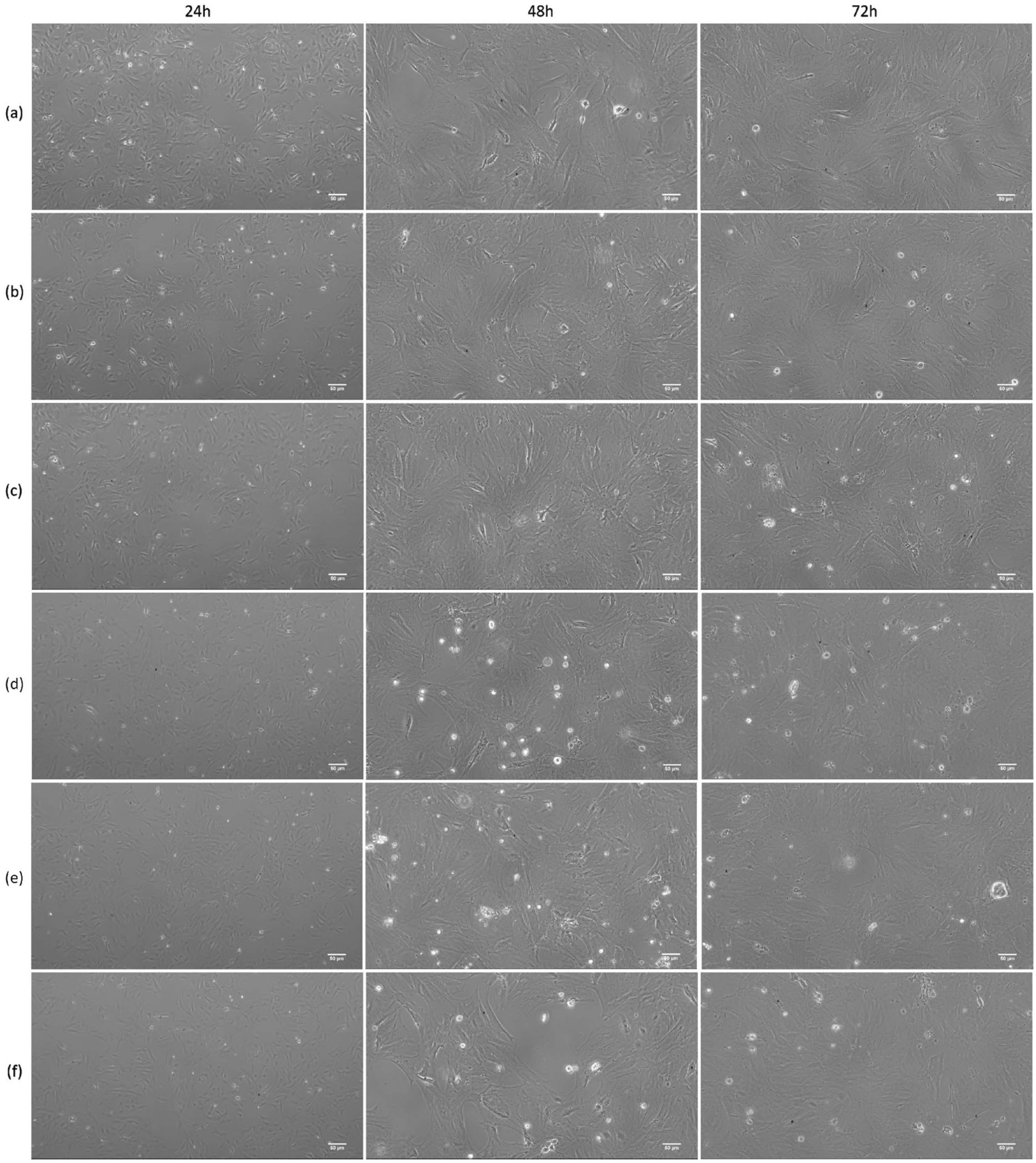

Fig. 4 Microscope images of mouse embryonic fibroblasts after 24, 48 and 72 h incubation on **a** control, **b** geopolymer, **c** geopolymer–CHA, **d** geopolymer–CHA–Mg, **e** geopolymer–CHA–Sr, and **f** geopolymer–CHA–Sr–Mg. The bar denotes 50 µm

for dental materials has not been widely studied. Our results showed that geopolymer and geopolymer–carbonated apatite with and without Mg and Sr trace elements are excellent candidates for dental materials as they demonstrate mechanical and in vitro biological properties that are suitable for dental restorative materials.

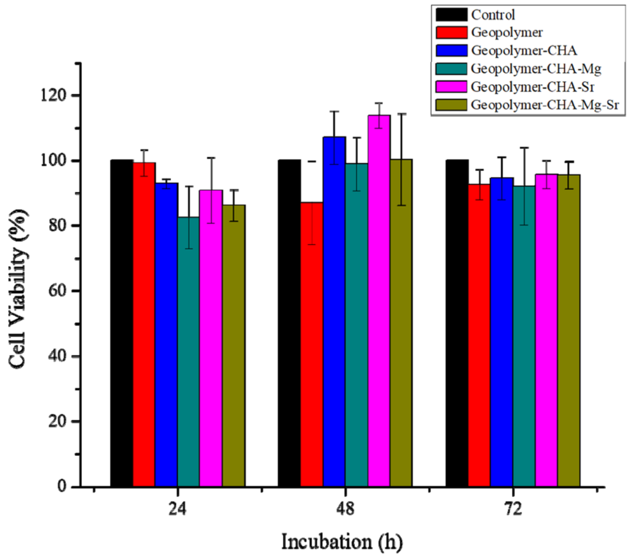

Fig. 5 Cell viability of embryonic fibroblasts on various samples after 24, 48 and 72 h incubation

4 Conclusions

The synthesis and mechanical properties of geopolymer–CHA nanocomposites with addition of Mg and Sr trace elements were studied. Although the hardness and modulus elasticity showed slight decrease after doping Mg and Sr, it was found that all samples reached the range of dentine hardness values. Geopolymer, geopolymer–CHA, and geopolymer–CHA–Mg–Sr nanocomposite reached the range values of enamel for compressive strength, tensile strength, and modulus elasticity properties. A replacement material for enamel should have a hardness value that is similar or lower than that of enamel; from the mechanical properties point of view, all samples are good candidate as replacement materials for enamel. Geopolymer–CHA nanocomposites showed modulus elasticity value that is suitable as a replacement material for both dentine and enamel. In this study, it was shown that the addition of minor elements did reduce the mechanical properties, but still could meet the requirements as a substitute for dentine or enamel. In our work, trace elements were added for the purpose of broader applications, one of which is for applications that require integration of cells. The cytotoxicity assay revealed that all samples were biocompatible toward fibroblast cells after 24, 48 and 72 h incubation. Assessment of incorporation of Mg and Sr in geopolymers–CHA nanocomposites toward cell integration is a crucial step that needs to be carried out in future works to investigate the role of these minor elements in vivo.

Acknowledgements This work was supported by the Ministry of Research, Technology, and Higher Education program (Kemenristekdikti) doctoral grant 2018 and Faculty of Dentistry of Maranatha Christian University. We thank Hernindya Dwifulqi for assistance with mechanical testing. L.A.T.W. A thanks to Community Service and Innovation Grant Program-ITB.

Compliance with ethical standards

Conflict of interest The authors declare no conflict of interest.

References

1. L. Wang, P.H.P. D'Alpino, L.G. Lopes, J.C. Pereira, Mechanical properties of dental restorative materials: relative contribution of laboratory tests. J. Appl. Oral Sci. **11**(3), 162–167 (2003)
2. M. Catauro, F. Bollino, F. Papale, Investigation of the sample preparation and curing treatment effects on mechanical properties and bioactivity of silica rich metakaolin geopolymer. Mater. Sci. Eng. **36**, 20–24 (2014)
3. L. Chen, Y. Wang, J. Feng, Preparation and properties of alkali activated metakaolin-based geopolymer. Materials **9**(9), 767 (2016)
4. P. Rovnanik, Effect of curing temperature on the development of hard structure of metakaolin-based geopolymer. Constr. Build Mater. **24**(7), 1176–1183 (2014)
5. I. Herwani, I. Pane, I. Imran, Budiono, Compressive strength of fly ash-based geopolymer concrete with a variable of sodium hydroxide (NaOH) solution molarity. Matec. Web. Conf. **147**, 1–5 (2018)
6. T.Z. BlaszczynskI, M.R. Krol, Alkaline activator impact on the geopolymer binders. IOP Conf. Ser. Mater. Sci. Eng. **245**(2), 2–11 (2017)
7. C. Tippayasam, C. Sutikulsombat, E. Kamseu, R. Rosa, P. Thavorniti, P. Chindaprasirt, C. Leonelli, G. Hennes, D. Chaysuwan, In vitro surface reaction in SBF of a non-crystalline aluminosilicate (geopolymer) material. Aust. Ceram. Soc. **55**, 11–17 (2019)
8. M. Catauro, F. Bollino, I. Kansal, L. Kamseu, L. Lancellotti, C. Lancelloti, C. Leonelli, Mechanical and biological characterization of geopolymers for potential application as biomaterials. Azo J. Mater. **5**, 1–15 (2012)
9. S. Okayama, M. Akao, S. Nakamura, Y. Shin, M. Higashikata, H. Aoki, Mechanical properties and solubility of strontium-substituted hydroxyapatite. Biomed. Mater. Eng. **1**(1), 11–17 (1991)
10. R.Z. Le Geros, R. Kijkowska, C. Bautista, J.P. Le Gores, Synergistic effect of magnesium and carbonate on properties of biological and synthetic apatite. Connect. Tissue Res. **33**(1–3), 203–209 (1995)
11. E. Landi, S. Sprio, M. Sandri, G. Celotti, A. Tampieri, Development of Sr and CO_3 co-substituted hydroxyapatites for biomedical applications. Acta Biomater. **4**(3), 656–663 (2008)
12. A.R. Boyd, L. Rutledge, D. Randolph, B.J. Meenan, Strontium-substituted hydroxyapatite coating deposited via a co-deposition sputter technique. Mater. Sci. Eng. C. **46**, 290–300 (2015)
13. F. Yang, D. Yang, J. Tu, Q. Zheng, L. Cai, L. Wang, Strontium enhances osteogenic differentiation of mesenchymal stem cells and in vivo bone formation by activating Wnt/catenin signaling. Stem Cells **6**(29), 981–991 (2011)
14. Z. Saidak, P.J. Marie, Strontium signaling: molecular mechanisms and therapeutic implications in osteoporosis. Pharmacol. Ther. **136**(2), 216–226 (2012)
15. E. Bresciani, T.D.T.J. Barata, T.C. Fagundes, A. Adachi, M.M. Terrin, M.F.D.L. Navarro, Compressive and diametral tensile strength of glass ionomer cements. J. Appl. Oral Sci. **12**(4), 344–348 (2004)

16. J. Wu, M.D. Weir, M.A.S. Melo, H.H.K. Xu, Development of novel of self healing and antibacterial dental composite containing calcium phosphate nanoparticles. J. Dent. **43**(3), 317–326 (2015)
17. J. Fishcher, B. Stawarczyk, C.H.F. Hemmerle, Flexural strength of the veneering ceramic for zirconia. J. Dent. **36**(5), 316–321 (2008)
18. R. Meshramkar, R. Mahajan, R. Nadiger, Evaluation of cytotoxicity of polyetheretherketone (PEEK) as a dental implant material. J. Dent. Oral Biol. **3**(2), 1–3 (2018)
19. E. Cal, V.B. Cetintas, H. Boyacioglu, P. Guneri, Cytotoxicity of dental implant the effect of ultrastructural element. Int. J. Oral Max. Impl. **32**(6), 1281–1287 (2017)
20. N. Kanasan, S. Adzila, H.A. Rahman, N. Bano, G. Panerselvan, N.A. Hidayati, FTIR and XRD evaluation of magnesium doped hydroxyapatite/sodium alginate powder by precipitation method. Key Eng. Mater. **791**, 45–49 (2018)
21. I. Rehman, W. Bonfield, Characterization of hydroxyapatite and carbonated apatite by photo acoustic FTIR spectroscopy. J. Mater. Sci. Mater. Med. **8**, 1–4 (1997)
22. V.F.F. Barbosa, K.J.D. Mac Kenzie, C. Thaumaturgo, Synthesis and characterisation of materials based on inorganic polymers of alumina and silica: sodium polysialate polymers. Int. J. Inorg. Mater. **2**(4), 309–317 (2000)
23. J. Davidovits, *Geopolymer chemistry & applications*, 3rd edn. (Institut Géopolymère Saint-Quentin, France, 2011)
24. A.A.S. Tigue, R.A.J. Malenab, J.R. Dungca, D.E.C. Yu, M.A.B. Promentilla, Chemical stability and leaching behavior of one-part geopolymer from soil and coal fly ash mixtures. Minerals. **8**(9), 411 (2018)
25. Z. Aly, E.R. Vance, D.S. Perera, J.V. Hanna, C.S. Griffith, J. Davis, D. Durce, Aqueous leachability of metakaolin-based geopolymers with molar ratios of Si/Al = 1.5–4. J. Nucl. Mater. **378**(2), 172–179 (2008)
26. K.J. Chun, H.H. Choi, J.Y. Lee, Comparison of mechanical property and role between enamel and dentin in human teeth. J. Dent. Biomech. **5**, 1–7 (2014)
27. G.W. Marshall, S.J. Marshall, J.H. Kinney, M. Balooch, The dentin substrate: structure and properties related to bonding. J. Dent. **25**(6), 441–458 (1997)
28. K.J. Chun, J.Y. Lee, Comparative study of mechanical properties of dental restorative materials and dental hard tissues in compressive loads. J. Dent. Biomech. **5**(8), 1–6 (2014)
29. G. Kumar, A. Shivrayan, Comparative study of mechanical properties of direct core build-up materials. Contemp. Clint. Dent. **6**(1), 16–20 (2015)
30. L. Jia, P. He, D. Jia, S. Fu, M. Wang, M. Wang, X. Duan, Z. Yang, Y. Zhou, Immobilization behavior of Sr in geopolymer and its ceramic product. J. Am. Ceram. Soc. **103**(2), 1372–1384 (2019)
31. B. Walkley, X. Ke, O.H. Hussein, S.A. Bernal, J.L. Provis, Incorporation of strontium and calcium in geopolymer gels. J. Hazard Mater. **382**, 4 (2019)